Determining receiver biases in GPS-derived total electron content in the auroral oval and polar cap region using ionosonde measurements

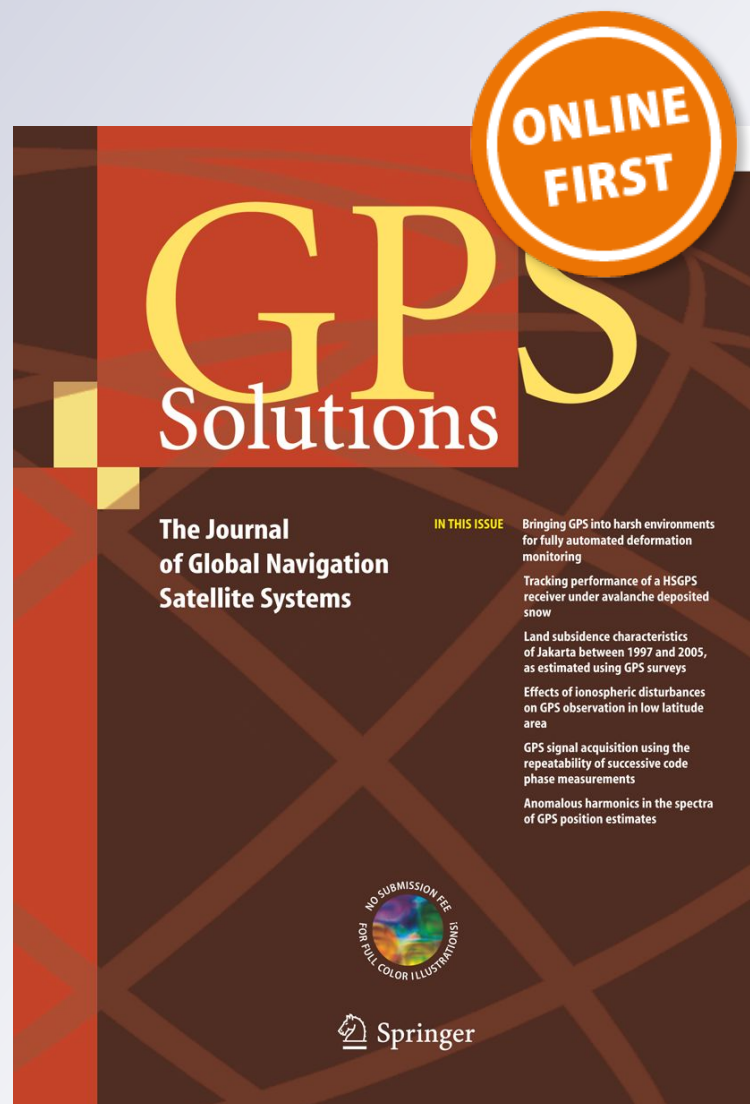# David R. Themens, P. T. Jayachandran, R. B. Langley, J. W. MacDougall & M. J. Nicolls

GPS
Solutions

The Journal
of Global Navigation
Satellite Systems

IN THIS ISSUE

Bringing GPS into harsh environments for fully automated deformation monitoring

Tracking performance of a HSGPS receiver under avalanche deposited snow

Land subsidence characteristics of Jakarta between 1997 and 2005, as estimated using GPS surveys

Effects of ionospheric disturbances on GPS observation in low latitude area

GPS signal acquisition using the repeatability of successive code phase measurements

Anomalous harmonics in the spectra of GPS position estimates

NO SUBMISSION FEE FOR FULL COLOR ILLUSTRATIONS

🐎 Springer

🐎 Springer

Springer

ORIGINAL ARTICLE

Determining receiver biases in GPS-derived total electron content in the auroral oval and polar cap region using ionosonde measurements

David R. Themens · P. T. Jayachandran · R. B. Langley · J. W. MacDougall · M. J. Nicolls

Abstract Global Positioning System (GPS) total electron content (TEC) measurements, although highly precise, are often rendered inaccurate due to satellite and receiver differential code biases (DCBs). Calculated satellite DCB values are now available from a variety of sources, but receiver DCBs generally remain an undertaking of receiver operators and processing centers. A procedure for removing these receiver DCBs from GPS-derived ionospheric TEC at high latitudes, using Canadian Advanced Digital Ionosonde (CADI) measurements, is presented. Here, we will test the applicability of common numerical methods for estimating receiver DCBs in high-latitude regions and compare our CADI-calibrated GPS vertical TEC (vTEC) measurements to corresponding International GNSS Service IONEX-interpolated vTEC map data. We demonstrate that the bias values determined using the CADI method are largely independent of the topside model (exponential, Epstein, and α-Chapman) used. We further confirm our results via comparing bias-calibrated GPS vTEC with those derived from incoherent scatter radar (ISR) measurements.

These CADI method results are found to be within 1.0 TEC units (TECU) of ISR measurements. The numerical methods tested demonstrate agreement varying from within 1.6 TECU to in excess of 6.0 TECU when compared to ISR measurements.

Introduction

The consistent availability and precision of Global Positioning System (GPS) total electron content (TEC) measurements makes GPS an asset in ionospheric research and applications; unfortunately, inherent receiver differential code biases (DCBs) can restrict the use of GPS TEC measurements to analyzing relative variations in TEC. It will be demonstrated that the reliability of previous methods for accounting for these DCBs may be questionable for the analysis of high-latitude observations. In order to increase the versatility of GPS TEC measurements, we must determine a reliable means of removing receiver DCBs from GPS-measured TEC for such observations.

TEC is commonly used as a means of investigating the nature of the ionosphere's variability and structure, and has become an increasingly important parameter in ionospheric research. It is defined as the total number of electrons within a 1-m^2 column along a path through the ionosphere. TEC is measured in TEC Units (TECU), where 1 TECU $= 10^{16}$ electrons/m^2 and can be determined via a variety of different means; the more pertinent to this study being via GPS, ionosonde, or incoherent scatter radar (ISR) observations.

D. R. Themens (✉) · P. T. Jayachandran
Department of Physics, University of New Brunswick, Fredericton, NB E3B 5A3, Canada
e-mail: david.themens@gmail.com

R. B. Langley
Department of Geodesy and Geomatics Engineering, University of New Brunswick, Fredericton, NB E3B 5A3, Canada

J. W. MacDougall
Department of Physics and Astronomy, University of Western Ontario, London, ON N6A 3K7, Canada

M. J. Nicolls
Center for Geospace Studies, SRI International, Menlo Park, CA, USA

GPS, primarily broadcasting two L-band frequencies (L1 = 1,575.42 and L2 = 1,227.60 MHz), provides a host of observables pertinent to ionospheric studies; those particularly important to TEC calculation include pseudorange and carrier phase measurements. Using these observables, one may calculate signal delays, which have been related to ionospheric TEC along the ray path of the GPS signal. Within the delays measured in this way, there reside inherent biases due to the satellite and receiver hardware involved (Warnant 1997; Arikan et al. 2008). These biases alter the level of the TEC measured by GPS receivers and serve as the main source of error in GPS TEC measurements. In order to determine absolute TEC, one must remove these biases by some reliable means.

Previous single-station methods for determining receiver DCBs often involve comparing GPS TEC to modeled TEC; unfortunately, due to a lack of available high-latitude observations, the models used are often calibrated, predominantly, by measurements at latitudes far lower than those with which we are concerned (Lanyi and Roth 1988; Ma and Maruyama 2003; Arikan et al. 2008). Due to this, we suspect that methods for DCB calculation that involve these models do not offer, at high latitudes, the accuracy they are shown to provide at lower latitudes. Other methods for DCB calculation often involve least-squares analysis based on assumptions that do not necessarily hold at high latitudes, such as the least-squares fitting to polynomials method outlined in Lanyi and Roth (1988), where the high variability of the polar and auroral ionosphere can conflict with assumptions related to the "temporal behavior of the ionosphere" (Lanyi and Roth 1988). Excluding the above two categories of receiver DCB estimation, there exist other, simple methods for determining receiver DCBs, such as the minimization of the standard deviation of GPS TEC measurements method presented by Ma and Maruyama (2003) and the pierce-point crossover methodology of Smith (2004).

The Canadian High Arctic Ionospheric Network (CHAIN) is devoted to achieving a greater understanding of the high-latitude ionosphere using, in part, GPS TEC measurements. CHAIN provides an array of instrumentation that can be used to study the ionosphere at high latitudes, including five Canadian Advanced Digital Ionosondes (CADIs) collocated with GPS receivers (Table 1) (Jayachandran et al. 2009). Due to this feature, one may test the reliability of these measuring systems against one another and calibrate their measurements appropriately; in particular, this arrangement allows for the reliable calculation of GPS DCBs in high-latitude regions using CADI-derived TEC, as is undertaken in this study.

In the "Measuring slant and vertical TEC with GPS" section, we will discuss how GPS TEC is calculated and how receiver DCBs affect these calculations. Our method

Table 1 List of stations with collocated CADI and GPS receivers

Station	Station synonym	Latitude	Longitude
Eureka	eurc	79.99°N	274.10°E
Resolute Bay	resc	74.75°N	265.00°E
Pond Inlet	ponc	72.69°N	282.04°E
Cambridge Bay	cbbc	69.12°N	254.97°E
Hall Beach	halc	68.78°N	278.74°E

for determining CADI TEC for comparison with GPS values is discussed in the "Determining CADI-derived slant TEC" section. The proposed method for receiver DCB estimation and some results of its application are presented in the "Receiver DCB estimation" section. In the "Discussion" section, the consistency of and methodology behind our CADI method is discussed along side that of two numerical DCB estimation techniques commonly used. A validation of our CADI method is undertaken in the "Validating the use of the CADI method" section, where bias-calibrated GPS TEC is compared with that derived from ISR measurements.

Measuring slant and vertical TEC with GPS

The time delay of GPS signals, including the effects of the ionosphere and instrumental biases measured by GPS receivers, is converted to pseudorange (code) values for both L-band frequencies via a conversion using the vacuum speed of light. The receiver also measures carrier phase for both frequencies. These pseudorange and carrier phase measurements can be described by the following:

$$P_1 = \rho_k^p + c(\mathrm{d}t^p - \mathrm{d}t_k) + I_{k,1,P}^p + T_k^p + c(d_{k,1} + d_1^p) \qquad (1)$$

$$P_2 = \rho_k^p + c(\mathrm{d}t^p - \mathrm{d}t_k) + I_{k,2,P}^p + T_k^p + c(d_{k,2} + d_2^p) \qquad (2)$$

$$L_1 = \rho_k^p + c(\mathrm{d}t^p - \mathrm{d}t_k) + I_{k,1,L}^p + T_k^p - c(\varphi_{k,1} - \varphi_1^p) + \lambda_1 N_{k,1}^p \qquad (3)$$

$$L_2 = \rho_k^p + c(\mathrm{d}t^p - \mathrm{d}t_k) + I_{k,2,L}^p + T_k^p - c(\varphi_{k,2} - \varphi_2^p) + \lambda_2 N_{k,2}^p \qquad (4)$$

as in Leick (2004), where P_f is the pseudorange measured on frequency f, L_f is the carrier phase measured on frequency f, ρ_k^p is the geometric range between receiver k and satellite p, $\mathrm{d}t^p$ and $\mathrm{d}t_k$ are, respectively, satellite and receiver clock errors, $I_{k,f,P}^p$ and $I_{k,f,L}^p$ are the ionospheric code delay and phase advance on signal f, respectively (in meters), T_k^p is the neutral atmosphere (tropospheric) delay (in meters), $d_{k,f}$ and d_f^p are, respectively, receiver and satellite hardware delays on signal f code measurements, $\phi_{k,f}$ and ϕ_f^p are, respectively, receiver and satellite

hardware delays on signal f phase measurements, λ_f is the wavelength of signal f, and $N_{k,f}^p$ is the integer phase ambiguity in signal f. It should be noted at this point that P_1, P_2, L_1, and L_2 have all been converted to units of meters in the above representative equations for the sake of simplicity; also, multipath and measurement noise are not explicitly noted in the equations.

Taking the difference of P_2 and P_1 as well as L_1 and L_2, we are left with

$$P_{k,\text{GF}}^p = P_2 - P_1 = I_{k,2,P}^p - I_{k,1,P}^p - \text{c}(\text{DCB}^p + \text{DCB}_k) \quad (5)$$

$$L_{k,\text{GF}}^p = L_1 - L_2 = I_{k,1,L}^p - I_{k,2,L}^p - \text{c}(\text{DPB}^p + \text{DPB}_k) + n_k^p \quad (6)$$

where $n_k^p = \lambda_1 N_{k,1}^p - \lambda_2 N_{k,2}^p$ and $\text{DCB}^p = d_1^p - d_2^p$, $\text{DCB}_k = d_{k,1} - d_{k,2}$, $\text{DPB}^p = \phi_1^p - \phi_2^p$, and $\text{DPB}_k = \phi_{k,1} - \phi_{k,2}$ are, respectively, satellite and receiver differential code and differential phase biases (in units of seconds) (Arikan et al. 2008). We have thus removed all frequency-independent terms, including the tropospheric and geometric unknowns. These difference equations are known as the geometry-free linear combinations of pseudorange and carrier phase, respectively, and can be related to slant TEC (sTEC), in TECU, along the ray path of the signal via the substitution of the following approximation, derivable from the Appleton-Hartree equation, into (5) and (6),

$$I_{k,f,P}^p = -I_{k,f,L}^p \approx A \frac{\text{sTEC}_k^p}{f^2} \quad (7)$$

where $A = 40.3$ and f is the signal frequency in MHz. Combining this with (5) and (6) yields two relations for determining sTEC via GPS observables

$$P_{k,\text{GF}}^p = A\left(\frac{f_1^2 - f_2^2}{f_1^2 f_2^2}\right)\text{sTEC}_k^p - \text{c}(\text{DCB}^p + \text{DCB}_k) \quad (8)$$

$$L_{k,\text{GF}}^p = A\left(\frac{f_1^2 - f_2^2}{f_1^2 f_2^2}\right) s\text{TEC}_k^p - \text{c}(\text{DPB}^p + \text{DPB}_k) + n_k^p \quad (9)$$

The sTEC determined from pseudorange measurements via the above relation contains no non-instrumental ambiguity but can be extremely noisy, while the sTEC determined from phase measurements via the above relation retains a phase ambiguity but is extremely precise. This phase ambiguity term must be removed if we are to capitalize on the high precision of phase measurements in our analysis. This is done by a phase-leveling procedure that effectively levels the phase-derived TEC to the pseudorange-derived TEC. The method used in our analysis is a similar procedure to those that can be found in Horvath and Crozier (2007), Arikan et al. (2008), and Makela et al. (2001). In this phase-leveling procedure, we first determine a leveling constant W

$$W = \frac{1}{N_{\text{arc}}} \sum_{N=1}^{N_{\text{arc}}} \left(P_{k,\text{GF}}^p - L_{k,\text{GF}}^p \right) \quad (10)$$

where N_{arc} is the total number of measurements over one arc of lock, and N is an epoch index. In order to minimize the effects of multipath and low elevation-angle noise in the estimation of the leveling constant, we limit the range considered in (10) to data acquired within 10° of the peak elevation angle of each arc. We can then substitute (8) and (9) into (10), resulting in

$$W = \langle \text{cDPB}_k^p \rangle - \langle \text{cDCB}_k^p \rangle - \langle n_k^p \rangle \quad (11)$$

where DPB_k^p and DCB_k^p simply represent the sum of the receiver and satellite biases in phase and pseudorange measurements, respectively. Since these DCBs and DPBs are considered constant over periods far longer than an arc (Sardón and Zarraoa 1997) and the integer ambiguity is constant over an arc, the terms in (11) can be taken such that

$$W = \text{cDPB}_k^p - \text{cDCB}_k^p - n_k^p \quad (12)$$

If we then rearrange (9) for sTEC and substitute in (12), we are left with

$$\text{sTEC}_k^p = \frac{1}{A}\left(\frac{f_1^2 f_2^2}{f_1^2 - f_2^2}\right)\left(L_{k,\text{GF}}^p + W + \text{cDCB}_k^p\right) \quad (13)$$

where the sTEC term can be taken as the phase-leveled sTEC. It should be noted that in this manner, the phase-leveled sTEC is independent of the DPB and n_k^p terms previously found in phase relation (9). Calculating W from (10) and removing the satellite biases, we are only left with a receiver DCB ambiguity in our values of measured GPS sTEC. Figure 1 demonstrates a sample of phase-leveled GPS sTEC, derived from this procedure, for all satellites in view during the period between September 16 and 24, 2009, at the Resolute CHAIN station in one-second resolution. For the remainder of this analysis, all references to GPS TEC are to be taken as references to GPS phase-leveled TEC.

For the purpose of comparison with ISR-derived vertical TEC (vTEC) values in the "Validating the use of the CADI method" section, we must convert GPS-derived sTEC to equivalent vTEC. We achieve this by first removing satellite DCBs from GPS-derived sTEC values, where P1–C1 and P1–P2 biases were retrieved from the University of Bern ftp database at ftp://ftp.unibe.ch/aiub/CODE/ and ftp://ftp.unibe.ch/aiub/BSWUSER50/ORB/, respectively. We then restrict the sTEC values to measurements made at satellite elevation angles greater than 30°, so as to minimize multipath effects, while also ensuring that GPS ray paths stay within the polar cap region through the plasmasphere, limiting the plasmaspheric contribution to
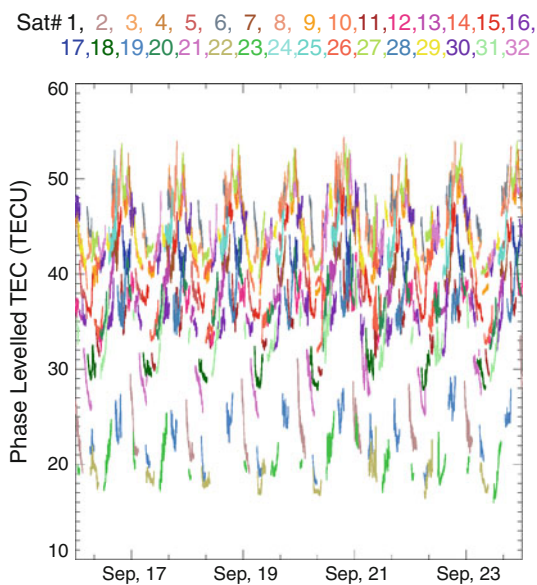
Sat# 1, 2, 3, 4, 5, 6, 7, 8, 9, 10,11,12,13,14,15,16,
17,18,19,20,21,22,23,24,25,26,27,28,29,30,31,32

Fig. 1 An example of raw, phase leveled, GPS-derived sTEC at the Resolute station for September 16–24, 2009

GPS-derived TEC. Following this, we map these GPS sTEC measurements to vTEC via a simple geometric mapping function derived via the single-layer ionosphere model (SLIM) (see Fig. 2)

$$\text{vTEC} = \text{sTEC} \cdot M(e) \tag{14}$$

where $M(e)$ is represented by the following relationship:

$$M(e) = \cos(\chi) = \sqrt{1 - \left(\frac{R\cos(e)}{R + h}\right)^2} \tag{15}$$

where R is the mean radius of the Earth, e is the elevation angle measured from the horizon at the receiver to the ray
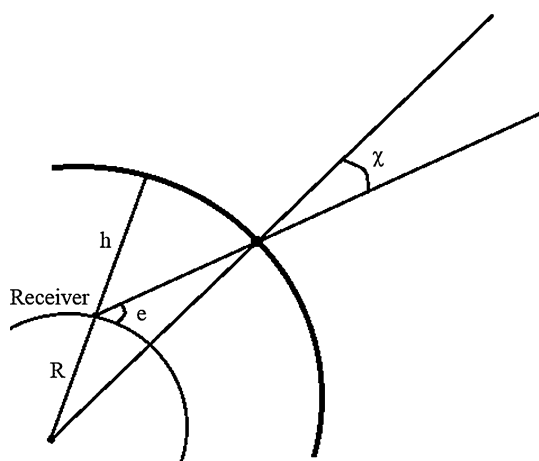

Fig. 2 Diagram of the geometry of the single-layer ionosphere model (see text for definitions)

from the satellite to the receiver, χ is the ray's zenith angle at the intersect of the ray and the ionospheric shell, and h is the ionospheric thin shell height (Gaussiran et al. 2004), derived from CADI measurements of the F_2 peak height as in Mushini et al. (2009). This mapping results in the determination of vTEC through the ionospheric pierce point (IPP), the point at which the ray from the satellite to the receiver intersects the thin shell ionosphere. If we assume that TEC gradients in the ionosphere are minimal in the region of study, the IPP vTEC can be approximated as the vTEC above the receiver. Understanding that assuming such is an idealization, we average the IPP vTEC, derived from the above mapping function, over all satellites in view, in order to minimize the effect of potential TEC gradients in the ionosphere. All references toward GPS vTEC in the remainder of this study should be taken as referring to this averaged, mapped GPS vTEC.

Determining CADI-derived slant TEC

In this study, absolute ionospheric TEC is derived from CADI vertical electron density profiles up to the F_2 peak of the ionosphere, above which the topside ionosphere is then modeled by an analytical profile derived using CADI parameters. CADI produces ionograms (frequency-height profiles) of ionospheric critical frequencies and associated virtual heights by sweeping through a frequency range from 1 to 20 MHz while timing echo signals reflected from the ionosphere (Davies 1990). The frequency at which the signal is reflected by the ionosphere can be related to electron density at the effective reflection height via (16), a relationship derived from the electron plasma frequency of the ionosphere.

$$N_e = \frac{\varepsilon_o m_e}{e^2}\omega^2 \tag{16}$$

where $\varepsilon_o = 8.85419e\text{-}12$ farad/m is the permittivity of free space, $m_e = 9.10938e\text{-}31$ kg is the rest mass of the electron, $e = 1.60218e\text{-}19$ C is the charge of an electron, and ω is the angular frequency at which the signal is reflected by the ionosphere.

The echo time delay for a particular reflected frequency is converted to a virtual height via a speed of light conversion. Due to the refractive index of the ionosphere, the virtual heights of reflection, determined via CADI, must be converted to real heights to account for delays due to the signal medium. This process is undertaken via the Polynomial Analysis (POLAN) method with manually scaled virtual height profiles as input (Titheridge 1985, 1988).

Ionograms are available in either 1- or 5-min temporal resolutions and 6-km altitude resolution from the CHAIN

network, depending on the station and time of study (all data after the summer of 2009 are at 1-min temporal resolution). Figure 3 demonstrates an example ionogram, displaying both the ordinary (black) and extraordinary (red) modes of reflection, along with their corresponding real height profiles, retrieved from CADI data corresponding to August 16, 2010, at 5:55 UT.

In order to determine the topside electron density profile, we use an α-Chapman topside model:

$$N_T = N_{F_2} \exp\left[\frac{1}{2}\left(1 - \left(\frac{h_o - h}{H}\right) - \exp\left(\frac{h_o - h}{H}\right)\right)\right]$$

(17)

where N_{F_2} is the electron density at the F_2-layer peak, h_o is the height of the F_2-layer peak, H is the CADI-derived scale height, and h is the height corresponding to electron density N_T. The α-Chapman is often used as a topside model since it is "more related to physics" (Warnant and Jodogne 1998), but quantitative justification for its use in our study is nonetheless presented in the "Discussion" section to demonstrate the consistency of our method. As plasmaspheric electron content is generally considered negligible at high latitudes, this topside profile is generated up to 1,000 km altitude and a plasmaspheric model is not implemented (Nsumei et al. 2008; Tu et al. 2004).

The real height electron density profiles returned from the POLAN procedure and the topside electron density profile, described above, are then interpolated to produce 76 12.5-km-thick, constant-density layers between 50- and 1,000-km altitude. We then apply a spherical shell model, as in Smith et al. (2008), to determine the slant content through each layer along the path of the GPS signal. The slant content in layer i is given by

$$\text{sTEC}_i = N_i \cdot \left[\sqrt{\left(r_i + \frac{d}{2}\right)^2 - r_i^2 \sin^2 \chi_i} - \sqrt{\left(r_i - \frac{d}{2}\right)^2 - r_i^2 \sin^2 \chi_i}\right]$$

(18)

where $r_i = R + h_i$ and h_i is the altitude of the spherical shell taken as the altitude at the middle of the ith layer, χ_i is the piercing angle of the GPS ray path through the layer, $d = 12.5$ km is the thickness of the ionospheric layer, and N_i is the electron density at the center of the layer. The total slant TEC, derived from CADI observations, along the GPS ray path is then simply the sum of the slant contents through each ionospheric layer (Smith et al. 2008). This procedure is undertaken for each satellite in view at elevations greater than 30°. An example of CADI-derived sTEC for all satellites in view corresponding to the same time period sampled in Fig. 1 is presented in Fig. 4.

Receiver DCB estimation

The simple and reliable method for receiver DCB estimation to be presented involves comparing GPS sTEC to that determined with CADI via a linear regression fit. We begin by isolating periods where three consecutive days of 5-min resolution or one full day of 1-min resolution GPS and CADI data are available at the site of interest. We then undertake the procedures presented in the "Measuring slant and vertical TEC with GPS" and "Determining CADI-derived slant TEC" sections to determine GPS and CADI sTEC values, where GPS satellite biases were removed prior to analysis. These sTEC values are then converted to a common temporal resolution (the temporal resolution of available CADI data) via a boxcar averaging of GPS sTEC values over the time period in which each ionosonde sweep was undertaken. An example plot of this satellite-bias-
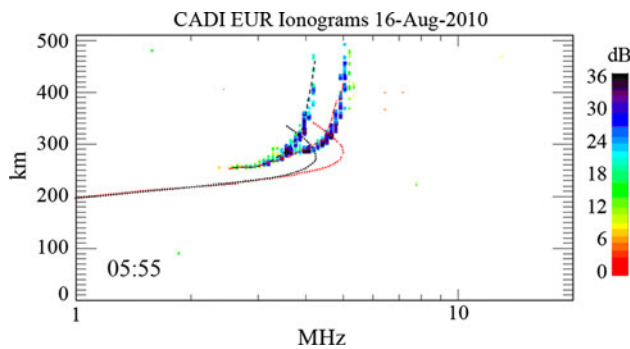

Fig. 3 A CADI ionogram at the Eureka site for August 16, 2010 at 5:55 UT. The *dashed black line* is a virtual height scaling of the ordinary mode, the *dashed red line* is a virtual height scaling of the extraordinary mode, and the *dotted lines* represent the corresponding real height profiles returned from POLAN
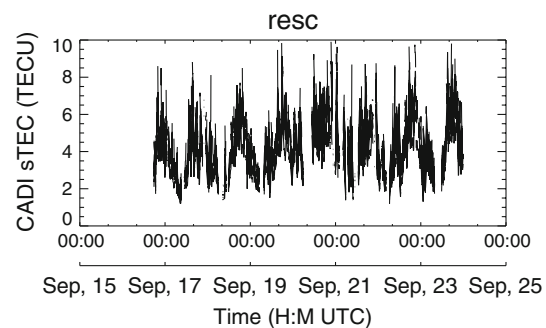

Fig. 4 An example of CADI-derived sTEC at the Resolute station for September 16–24, 2009, corresponding to the GPS-derived sTEC shown in Fig. 1. Ionograms used in this figure were available in 5-min resolution
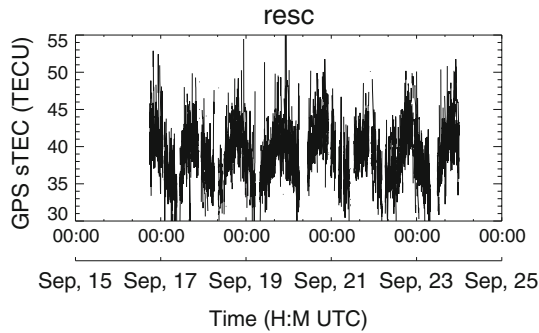
Fig. 5 An example of satellite-bias-corrected GPS sTEC, in 5-min resolution, at the Resolute station for September 16–24, 2009

Fig. 6 GPS sTEC plotted against CADI-derived sTEC at the Resolute station for September 16–24, 2009

corrected GPS sTEC, for all satellites in view, corresponding to the same time period sampled in Figs. 1 and 4 is presented in Fig. 5. Finally, GPS sTEC values are plotted against CADI sTEC values and a linear regression is performed, where the y-intercept value of the linear fit of GPS sTEC to CADI sTEC is interpreted as the receiver DCB value corresponding to the station in question. This y-intercept value, and effectively the receiver DCB value, is calculated via the following relation:

$$
\begin{aligned}
&\text{TECDCB}_k \\
&= \frac{\sum \text{CTEC}^2 \sum \text{GTEC} - \sum \text{CTEC} \sum (\text{GTEC} \cdot \text{CTEC})}{N \sum \text{CTEC}^2 - (\sum \text{CTEC})^2}
\end{aligned}
\tag{19}
$$

where TECDCB_k is the receiver DCB in TECU, CTEC is CADI-derived sTEC, GTEC is satellite-bias-corrected GPS-measured sTEC, and N is the number of measurements made over the entire measurement period (Taylor 1997). Figure 6 demonstrates the relationship between GPS and CADI sTEC corresponding to the example days shown in Figs. 1 and 4. From this figure, it can be seen that TEC determined by the two methods agrees well (correlation coefficient 0.55) and demonstrates a y-intercept determined receiver bias value of 33.28 ± 0.10 TECU. We have applied the same technique to the remaining CHAIN stations listed in Table 1 and plotted the results in Fig. 7. From these figures, it can be seen that DCBs varied between ∼33 and 36 TECU.

Discussion

Before a thorough evaluation of the CADI method can be undertaken, one must consider the potential shortcomings of such a method as well as any dissimilarity with prior techniques. For the CADI method, primary concerns can be associated with the topside model selected. In order to account for such concerns, we shall demonstrate the
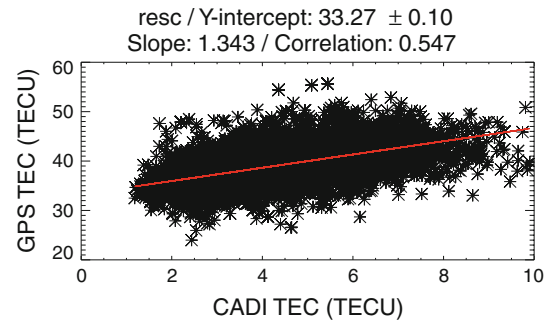
measures that were undertaken in order to minimize the influence of the topside model on our bias results.

Often DCB estimation methods use a comparison technique derived using relation (8) in determining DCB values:

$$
\text{DCB}_k = \text{GTEC} - \text{CTEC} - \text{DCB}^p
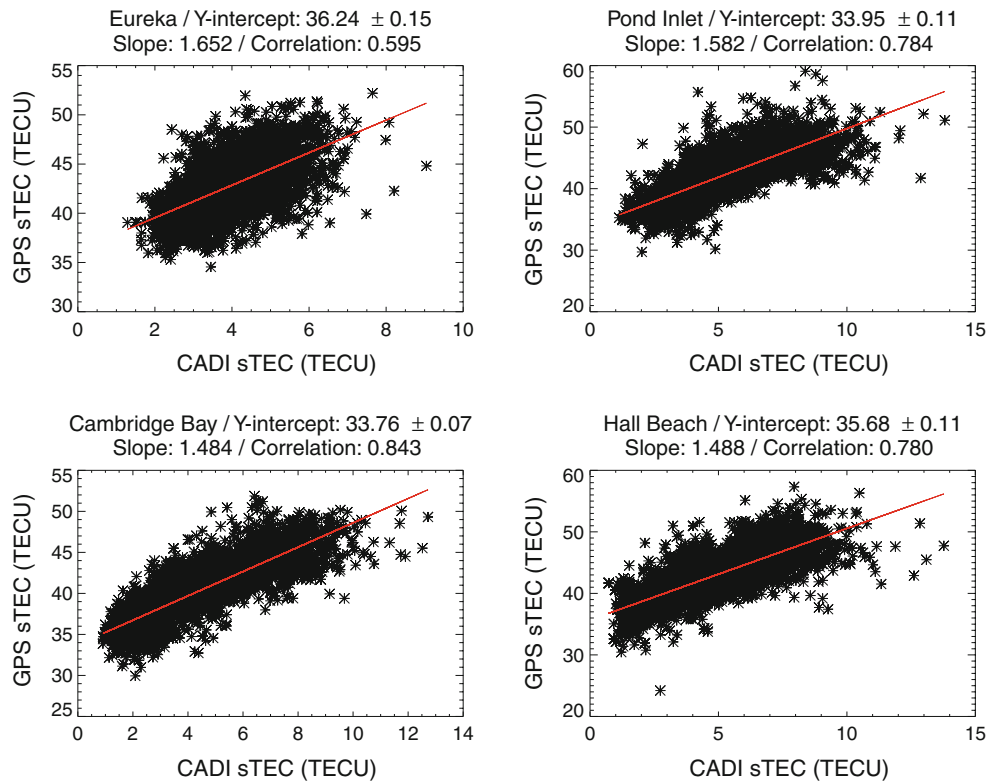\tag{20}
$$

where CTEC is taken as a reference TEC measurement and all parameters are given in TECU.

A linear regression is undertaken in place of using relation (20) in order to minimize the shortcomings of the topside model chosen. To elaborate, if, in fact, a topside model could be chosen in such a way as to guarantee the one-to-one relationship between GPS and CADI vTEC, both the linear fit method and a method using (20) to determine receiver DCBs would yield identical results. With a potentially inadequate topside model, artificial diurnal variations in the receiver DCBs determined via (20) bias the daily-determined DCB values (Wilson and Mannucci 1993). Using a linear fit, the choice of topside model will be demonstrated to have an ignorable effect on receiver DCBs determined in this manner, where methods using (20) would demonstrate artificial biases based on the choice of topside model.

Selecting a topside electron density profile

The choice of a topside electron density profile is expected to have a large impact on CADI-derived vTEC and thus must be considered before the reliability of the CADI bias estimation method outlined in the "Receiver DCB estimation" section can be demonstrated conclusively. In our analysis, we use three common topside models: the Epstein, exponential, and α-Chapman. Effectively, we compare the effects each topside model has on the bias value determined via the CADI method. We achieve this by merely substituting in different topside models prior to interpolating the CADI-derived electron density profiles in the procedure outlined in the "Determining CADI-derived slant TEC" section. We then compare the bias values

Fig. 7 Examples of GPS sTEC plotted against CADI-derived sTEC above CHAIN's Eureka, Pond Inlet, Cambridge Bay, and Hall Beach stations at various times in 2009

determined, where the $1 - \sigma$ statistical error in these bias values can be obtained via (21).

$$\delta_{\text{Bias}} = \sqrt{\frac{\left(\sum \text{CTEC}^2\right) \sum_{i=1}^{N} \left(\text{GTEC}_i - \text{TECDCB}_k - S \cdot \text{CTEC}_i\right)^2}{(N-2)\left(N \sum \text{CTEC}^2 - \left(\sum \text{CTEC}\right)^2\right)}}$$

(21)

where S is the slope of the line of best fit (Taylor 1997). Comparing the biases corresponding to each topside model and their associated error, we hoped to gauge the effect different topside models have on the CADI method. We then repeated this process for all of our stations and for varying times of a particular year. Some results of this analysis are presented in Table 2 and are demonstrated in Fig. 8, where we have also included the mean differences between CADI-derived and bias-corrupted GPS-derived sTEC.

From our observations, the bias values determined in this manner are found to be within the estimated 1-sigma error of one another. Thus, through this analysis, we have concluded that the bias obtained from our method is largely independent of the topside electron density profile chosen. Nonetheless, the model closest to achieving the expected one-to-one relationship between GPS and CADI sTEC values (GPS sTEC vs. CADI sTEC slope = 1.00) is

demonstrated to be the α-Chapman function, which is consistent with previous results in Mushini et al. (2009).

To demonstrate the need for the CADI method in high-latitude studies that use GPS measurements, we will present results from two common numerical bias estimation techniques: one involving least-squares fitting to a polynomial and the other using the standard deviation of vTEC measurements.

Minimization of standard deviations method

The minimization of standard deviations method, proposed by Ma and Maruyama (2003), is based on the assumption that the vTEC derived from each satellite in view should be identical if our assumptions with regard to the mapping function to determine vTEC are adequate and if receiver and satellite DCBs are properly removed. In this method, we determine the standard deviation of vTEC values derived from sTEC measurements from each satellite in view (above 30° elevation) while iteratively removing sample receiver DCBs from sTEC measurements before mapping sTEC to vTEC. That is, in the procedure discussed in the "Measuring slant and vertical TEC with GPS" section, in place of averaging vTEC values generated from each satellite, we determine the standard deviation of these vTEC values as in the following

Table 2 Comparison of CADI-method-derived receiver bias values and mean differences using different topside models

Station	Bias (TECU)	Error (TECU)	Slope	Mean differences (TECU)	Error (TECU)
eurc	36.24	0.15	1.65	38.82	0.04
	36.25	0.15	2.03	39.56	0.04
	36.20	0.15	2.86	40.47	0.04
resc	34.08	0.15	1.27	35.33	0.05
	34.12	0.15	1.55	36.19	0.05
	34.18	0.15	2.12	37.24	0.05
ponc	33.95	0.11	1.58	36.93	0.05
	33.97	0.11	1.94	37.89	0.05
	33.99	0.11	2.68	39.05	0.05
cbbc	33.76	0.07	1.48	35.81	0.04
	33.72	0.07	1.79	36.58	0.04
	33.83	0.07	2.39	37.52	0.04
halc	35.68	0.11	1.49	37.98	0.05
	35.72	0.11	1.82	38.85	0.05
	35.77	0.11	2.49	39.91	0.05

Values for each station are presented for each topside model in order of α-Chapman, Epstein, and Exponential
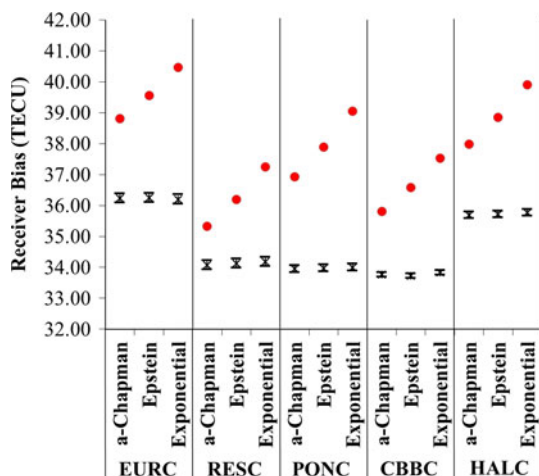

Fig. 8 Example demonstrating the agreement between biases estimated with the use of different topside models for the October 1–3, 2009 period. Also, plotted in are the mean differences between uncalibrated GPS- and CADI-derived sTEC for the same data

$$\sigma_k^b(t) = \sqrt{\frac{1}{P-1} \sum_{n=0}^{p} \left(\mathrm{GTEC}_k^p(t) - \overline{\mathrm{GTEC}}_k(t) \right)^2} \qquad (22)$$

where $\sigma_k^b(t)$ is the standard deviation at time t for station k and test bias b, and P is the total number of satellites in view at time t (Arikan et al. 2008). We then sum these standard deviations over the total number of sample measurements in the measuring period, as in (23).

$$\sigma_{k,\mathrm{total}}^b = \sum_{t=t_o}^{T} \sigma_k^b(t) \qquad (23)$$

where $\sigma_{k,\mathrm{total}}^b$ is the total standard deviation, t_o is the start time of the test period, and T is the end time of the test period. It is interesting to note at this point that propagation of variances would dictate the use of the summation of variances rather than the sum of standard deviations in (23). Also, one should account for the variability in the number of satellites in view by applying a method of pooled variances. Not accounting for these two factors could lead to potential errors in the DCBs estimated by this method and will be investigated in future work. Nonetheless, we apply the method as presented by the author and repeat this process for sample DCBs from 0.0 to 50.0 TECU in steps of 0.1 TECU. Finally, we determine the bias value at which $\sigma_{k,\mathrm{total}}^b$ is minimum. This value is taken as the receiver DCB (Ma and Maruyama 2003). An example of $\sigma_{k,\mathrm{total}}^b$ versus sample DCBs is presented in Fig. 9 for Resolute on September 19, 2009. In Fig. 9, the minimum is identified and the bias is determined as 34.8 TECU.

Least-squares fit to a polynomial method

The least-squares method for determining receiver and satellite DCBs was first introduced by Lanyi and Roth (1988). The method used in our analysis is a revised version of Lanyi and Roth's proposed method and is most closely presented in Coco et al. (1991) or Arikan et al. (2008). In this method, we make three primary assumptions with regard to the ionosphere and vTEC measurements:

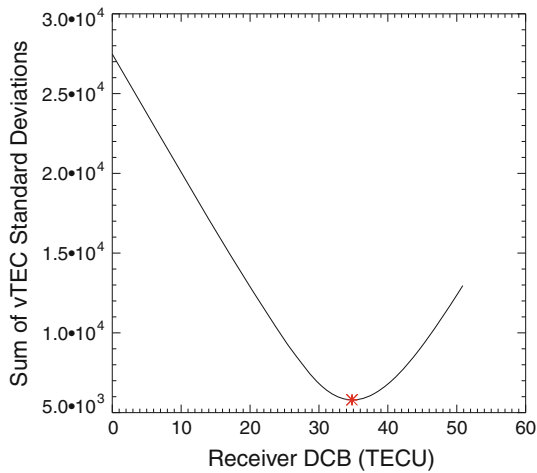- TEC is assumed to be independent of time in a reference frame fixed to the Sun-Earth vector.

Fig. 9 An example plot of the sum of SD versus sample biases for a 1-day sampling period on September 19, 2009 at the Resolute station. The *red star* indicates the minimum sum of SD, which corresponds to a receiver DCB value of 34.8 TECU

- The SLIM and function for mapping GPS sTEC to vTEC is assumed to hold over the sampling period chosen.
- GPS hardware biases are assumed to be constant over the time of the test period.

(Lanyi and Roth 1988)

Under the above assumptions, we attempt to fit GPS-derived vTEC to a second-order bivariate polynomial in IPP latitude and longitude outlined in the following relation:

$$vTEC = c_1 + c_2\lambda + c_3\phi + c_4\lambda^2 + c_5\phi\lambda + c_6\phi^2 \qquad (24)$$

where c_1 through c_6 are coefficients to be determined by a least-squares fit, λ is the IPP east longitude and ϕ is the IPP latitude (Lanyi and Roth 1988). These IPP coordinates are referenced to the Sun-Earth axis in a co-rotating frame, where the Sun is kept at 180°. Relations for converting GPS azimuth and elevation angle data into the IPP coordinates are presented in Lanyi and Roth (1988) and Gaussiran et al. (2004), while a simple means of transforming coordinate frames, used in our analysis, is presented in Coco et al. (1991).

It is taken as appropriate, given (24) and our assumptions, that satellite-bias-corrected sTEC can be modeled as

$$sTEC = DCB_k$$
$$+ M(e)\left(c_1 + c_2\lambda + c_3\phi + c_4\lambda^2 + c_5\phi\lambda + c_6\phi^2\right) \qquad (25)$$

where $M(e)$ is the mapping function outlined in (15). In order for the above to hold, the coefficients in (24) and (25), as well as the receiver and satellite DCBs, must remain constant over the course of the test period with which we are concerned. As discussed in Lanyi and Roth (1988), these

coefficients can be interpreted as constant if test periods are separated into individual nighttime and daytime tests. Concerning the stability of delays associated with receiver and satellite hardware, receiver and satellite DCBs have been shown in the past to remain sufficiently constant over significant spans of time (Sardón and Zarraoa 1997).

In this method, we fit GPS sTEC observations to (25), from which we derive a receiver DCB value for each test period. In order to insure the stability of the polynomial coefficients and receiver DCBs in our analysis, we have broken the typical test period into 2-h subset periods that overlap by 1 h. We then averaged receiver DCB values for each subset over the test period in order to get a representative DCB value for the period. In order to minimize multipath effects and the effects of gradients in the ionosphere, only data acquired above elevation angles of 30° are used in this analysis.

The application of these DCB estimation methods for high-latitude observations is presented in the following section where we will discuss the validity of these numerical techniques as well as that of the CADI method. This validation will be undertaken via a comparison with incoherent scatter radar (ISR) observations.

Validating the use of the CADI method

In order to justify the accuracy of our method against that of the numerical methods presented, we make use of ISR measurements made in a limited number of experiments at the Advanced Modular Incoherent Scatter Radar (AMISR) in Resolute, which is within 2 km of the Resolute CHAIN station. The Resolute AMISR uses the principle of Thomson Scattering to determine electron density profiles for various beam angles up to altitudes of 700 km (Davies 1990). In order to account for the 700-km altitude limit of these profiles, each profile is least-squares fit to a Chapman layer function so as to extrapolate up to 1,000 km. For our comparison, we integrate ISR-derived electron density profiles, retrieved from beam angles above 75° elevation, with their associated Chapman extrapolated profile in order to determine vTEC above the station. This ISR vTEC is compared with receiver DCB-calibrated GPS vTEC for the same period via a linear regression fit of GPS vTEC to ISR vTEC. The y-intercept of this fit is interpreted as an additional bias from the receiver bias at the Resolute station. An example of this fit is presented in Fig. 10. Comparison of results with DCBs determined using all methods discussed previously is undertaken for varying time periods at the Resolute station and is summarized in Table 3.

Table 3 demonstrates that the CADI method of calibration of GPS vTEC is consistently in good agreement with ISR-derived vTEC (within 1 TECU, or ∼0.53 ns, of
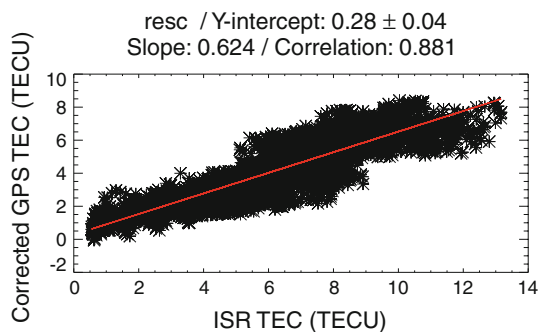
Fig. 10 An example of GPS sTEC against ISR sTEC for the September 15–23, 2009, experiment run at Resolute

ISR-measured DCBs). These differences between calibrated GPS and ISR-derived vTEC are well within the errors commonly accepted in other studies of this nature, which are typically in the range of 0.5 ns (Coco et al. 1991; Wilson and Mannucci 1993; Ma et al. 2005). Also, the GPS vTEC calibrated using the biases estimated via the two numerical methods presented in our analysis demonstrates, in Table 3, varying error from ISR-derived vTEC at the high-latitude Resolute station (y-intercepts between ISR- and GPS-derived vTEC at times in excess of 6 TECU, or $\sim$3.2 ns). In particular, the minimization of standard deviations method-calibrated GPS vTEC demonstrates fair agreement with ISR vTEC, where y-intercepts varied between -1.5 and -3.0 TECU. The least-squares method demonstrates more significant deviation in the form of a variable overestimation of the receiver bias, yielding y-intercepts varying from -2.1 to -6.4 TECU.

In order to offer a more complete view of the application of both the CADI method and the numerical methods presented, we have applied these methods at five CHAIN

stations for the period of October 1–3, 2009. The results of this analysis are presented in Table 4. As can be seen, both numerical methods demonstrate instances of significant deviation from CADI-derived receiver DCB values.

Based on the results presented in Tables 3 and 4, it becomes apparent that the least-squares method is inadequate for the analysis of high-latitude observations. This is somewhat expected, as the validity of the assumptions with regard to the "temporal behavior of the ionosphere" (Lanyi and Roth 1988), made in undertaking the least-squares method, become questionable for a highly dynamic and magnetically coupled region, such as the polar cap. The use of a magnetically defined coordinate system in these regions may result in the more reliable use of this method and is being investigated. As for the minimization of standard deviations method, errors could be attributed to the method of propagating variances applied in this method, the mapping function used, or potentially even to the absence of physically relevant weights in the summation of the standard deviations. Nonetheless, it is clear from these results that current receiver bias estimation techniques should be carefully reviewed in their application to these regions and that it is essential that alternative receiver DCB estimation methods, such as the CADI method, be investigated.

Further justifying the need for a reliable DCB estimation method at high latitudes, we have undertaken a comparison between CADI-method-calibrated GPS-derived vTEC and International GNSS Service (IGS) Ionosphere Map Exchange Format (IONEX) map data retrieved from the IGS global data center ftp server at the Goddard Space Flight Center (ftp://cddis.gsfc.nasa.gov/gps/products/ionex/). In order to facilitate comparison, we have produced vTEC data in the same temporal resolution as IGS map data via undertaking a 1-min boxcar mean about the time stamp of

Table 3 Y-intercepts of calibrated GPS vTEC versus ISR vTEC using each bias estimation method at resolute

Experiment date	09/16–23/09	10/15–18/09	11/05–07/09	12/04–08/09	02/01–07/11	02/9–11/11
CADI method (TECU)	0.28	-0.39	-0.36	-0.47	-0.22	0.19
Least-squares Method (TECU)	-6.39	-3.55	-3.43	-2.12	-6.19	-3.84
Min. SD method (TECU)	-2.08	-2.20	-2.38	-1.58	-2.96	-2.35

Table 4 Comparison between the methods presented for October 1–3, 2009, at all stations

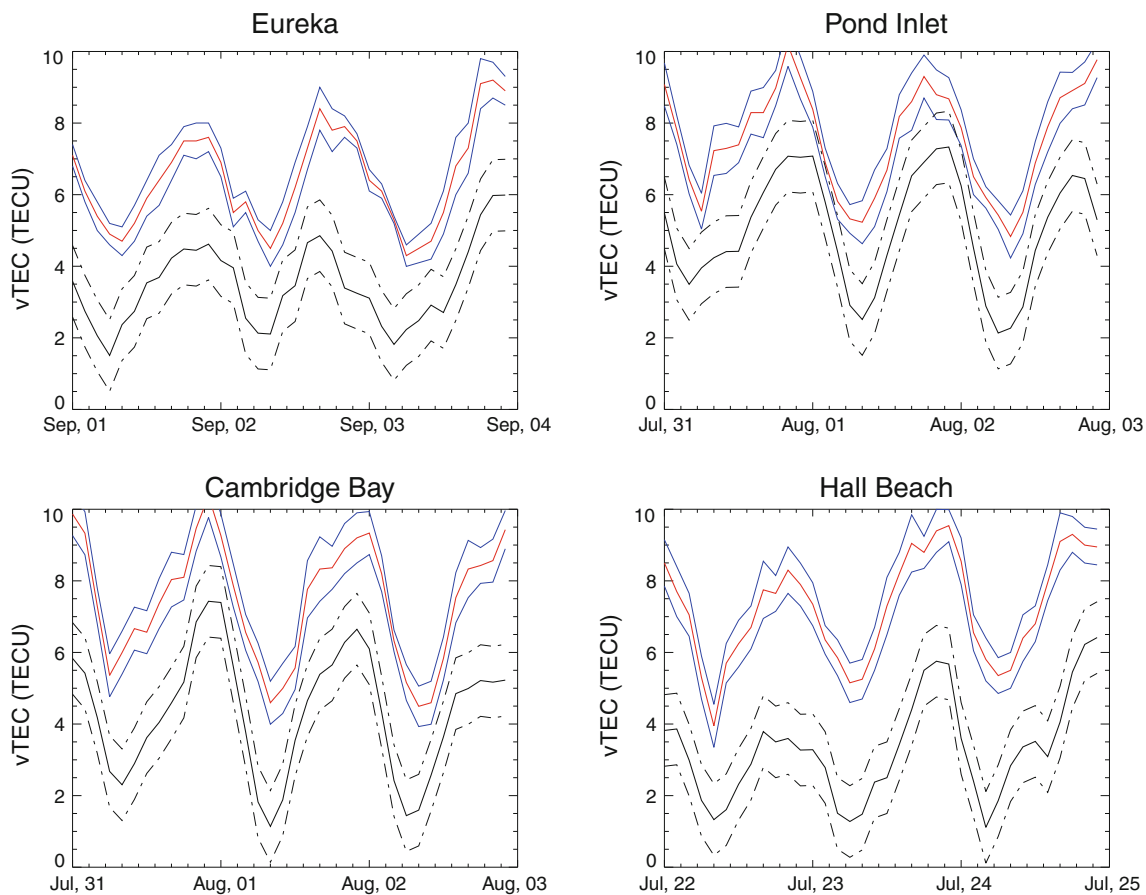| Letter	DCB estimation method	EURC	RESC	PONC	HALC	CBBC
A	CADI Method (TECU)	36.24	34.08	33.95	35.68	33.76
B	Least-squares method (TECU)	38.98	37.79	39.31	38.77	38.37
C	Min. SD method (TECU)	37.00	36.10	36.60	35.50	33.20
	A–B	-2.74	-3.71	-5.36	-3.09	-4.61
	A–C	-0.76	-2.02	-2.65	0.18	0.56

Fig. 11 An example of CADI-calibrated GPS-derived vTEC and IGS IONEX map vTEC above CHAIN's Eureka, Pond Inlet, Cambridge Bay, and Hall Beach stations at various times in 2009. The *red solid line* represents the IGS map vTEC, the *blue solid line* represents the

RMS error in IGS map vTEC, the *black solid line* represents the CADI-calibrated GPS-derived vTEC, and the *black segmented line* represents the SE in GPS-derived vTEC

each IGS data point. The results of this analysis for various time periods in 2009 are presented in Figs. 11 and 12. Figure 11 demonstrates that the IGS product is consistently overestimating vTEC values above the Eureka, Hall Beach, Pond Inlet, and Cambridge Bay stations, compared to our calibrated measurements. This was initially suspected to be the result of unaccounted for plasmaspheric content above the stations during our CADI calibration procedure. But upon the analysis of the data acquired from our Resolute station, this hypothesis has been refuted. Figure 12 demonstrates good agreement between IGS- and GPS-derived vTEC values, where this difference between results at the Resolute station and those from our remaining stations can be attributed to the fact that there is an IGS station in Resolute less than 2 km from the CHAIN station. Thus, since a discrepancy due to plasmaspheric content would persist at all stations, no matter their proximity to IGS stations, we may rule out plasmaspheric content as a source of error in the CADI DCB estimation method for high-latitude observations. Further research is needed in order to test the reliability of IGS IONEX-interpolated map data in
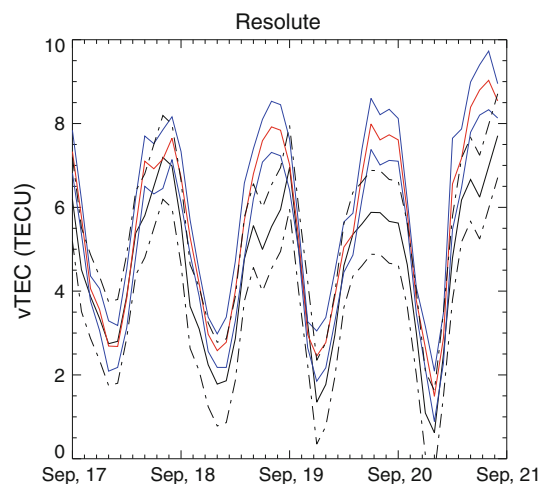

Fig. 12 An example of CADI-calibrated GPS-derived vTEC and IGS IONEX map vTEC above CHAIN's Resolute station between September 17 and 20, 2009. The *red solid line* represents the IGS map vTEC, the *blue solid line* represents the RMS error in IGS map vTEC, the *black solid line* represents the CADI-calibrated GPS-derived vTEC, and the *black segmented line* represents the SE in GPS-derived vTEC

its application to these high-latitude regions, but preliminary results suggest that these products are insufficient for these regions. This would exemplify the need for the incorporation of more high-latitude GPS stations into the IGS network.

Conclusion

We have demonstrated the capability of an ionosonde-based method for determining GPS receiver biases. The CADI-method-derived biases are seen to be independent of the topside model chosen. GPS vTEC, calibrated with the CADI method, demonstrates good agreement (within 1 TECU) with ISR-derived vTEC for the measurement periods available from the Resolute ISR. Numerical DCB estimation methods, namely the minimization of standard deviation and least-squares fit methods, are demonstrated to be have varying reliability in their application in high-latitude regions, exhibiting differences from ISR and CADI observations at times in excess of 6 TECU at the stations considered. It can be concluded, based on the results presented, that the use of the CADI method for estimating receiver DCBs is in fact justified in its use for determining GPS absolute TEC in high-latitude regions and, based on our results with regard to the IGS IONEX TEC maps, is necessary for determining accurate absolute TEC in these regions.

References

Arikan F, Nayir H, Sezen U, Arikan O (2008) Estimation of single station interfrequency receiver bias using GPS-TEC. Radio Sci 43:RS4004. doi:10.1029/2007RS003785

Coco DS, Coker C, Dahlke SR, Clynch JR (1991) Variability of GPS satellite differential group delay biases. IEEE Trans Aerosp Electron Syst 27(6):931–938

Davies K (1990) Ionospheric radio IEE electromagnetic waves series 31. Peter Peregrinus Ltd., London

Gaussiran T, Munton D, Harris B et al (2004) An open source toolkit for GPS processing, total electron content effects, measurements and modeling. In: Proceedings of the international Beacon symposium, Trieste, Italy

Horvath I, Crozier S (2007) Software developed for obtaining GPS-derived total electron content values. Radio Sci 42. doi:10.1029/2006RS003452

Jayachandran PT, et al (2009) Canadian high arctic ionospheric network (CHAIN). Radio Sci 44:RS0A03. doi:10.1029/2008RS004046

Lanyi GE, Roth T (1988) A comparison of mapped and measured total ionospheric electron content using Global Positioning System and beacon satellite observations. Radio Sci 23:483–492

Leick A (2004) GPS satellite surveying, 3rd edn. Wiley, Hoboken

Ma G, Maruyama T (2003) Derivation of TEC and estimation of instrumental biases from GEONET in Japan. Ann Geophys 21:2083–2093

Ma XF, Maruyama T, Ma G, Takeda T (2005) Determination of GPS receiver differential biases by neural network parameter estimation method. Radio Sci 40:RS1002. doi:10.1029/2004RS003072

Makela JJ, Kelley MC, Sojka JJ, Pi X, Mannucci AJ (2001) GPS normalization and preliminary modeling results of total electron content during a midlatitude space weather event. Radio Sci 36:351–361

Mushini SC, Jayachandran PT, Langley RB, MacDougall JW (2009) Use of varying shell heights derived from ionosonde data in calculating vertical total electron content (TEC) using GPS—new method. J Adv Space Res 44:1309–1313. doi:10.1016/j.asr.2009.07.015

Nsumei PA, Reinisch BW, Song P, Tu J, Huang X (2008) Polar cap electron density distribution from IMAGE radio plasma imager measurements: empirical model with the effects of solar illumination and geomagnetic activity. J Geophys Res 113:A01217. doi:10.1029/2007JA012566

Sardón E, Zarraoa N (1997) Estimation of total electron content using GPS data: how stable are the differential satellite and receiver instrumental biases? Radio Sci 32(5):1899–1910. doi:10.1029/97RS01457

Smith D (2004) Computing unambiguous TEC and ionospheric delays using only carrier phase data from NOAA's CORS network. In: Proceedings of IEEE position location and navigation symposium (PLANS) 2004, Monterey, California, 26–29 April 2004, pp 527–537

Smith DA, Araujo-Pradere EA, Minter C, Fuller-Rowell T (2008) A comprehensive evaluation of the errors inherent in the use of a two-dimensional shell for modeling the ionosphere. Radio Sci 43:RS6008. doi:10.1029/2007RS003769

Taylor JR (1997) An introduction to error analysis, 2nd edn. University Science books, Mill Valley

Titheridge JE (1985) Ionogram analysis: least-squares fitting of a Chapman layer peak. Radio Sci 20(2):247–256

Titheridge JE (1988) The real height analysis of ionograms: a generalized formulation. Radio Sci 23(5):831–849

Tu J-N, Horwitz JL, Nsumei PA, Song P, Huang X-Q, Reinisch BW (2004) Simulation of polar cap field-aligned electron density profiles measured with the IMAGE radio plasma imager. J Geophys Res 109:A07206. doi:10.1029/2003JA010310

Warnant R (1997) Reliability of the TEC computed using GPS measurements—the problem of hardware biases. Acta Geod Geophys Hung 32(3–4):451–459

Warnant R, Jodogne JC (1998) A Comparison between the TEC Computed using GPS and Ionosonde Measurements. Acta Geod Geophys Hung 33(1):147–153

Wilson BD, Mannucci AJ (1993) Instrumental biases in ionospheric measurements derived from GPS data. In: Proceedings of ION GPS-93, Salt Lake City, UT, 22–24 September, The Institute of Navigation, Alexandria, VA, pp 1343–1351

Author Biographies

David Themens is a Masters candidate in the Department of Atmospheric and Oceanic Sciences at McGill University, Montreal, Canada. His main research focuses on high-latitude ionospheric

remote sensing and instrument synergy. He has a B.Sc. in Physics from the University of New Brunswick, Canada.

P. T. Jayachandran is a professor of physics at the University of New Brunswick. His research focuses on the coupling processes in the solar wind—magnetosphere—ionosphere system. He is the principal investigator of the Canadian High Arctic Ionospheric Network (CHAIN), a ground-based network of GPS receivers and Canadian Advanced Digital Ionosondes deployed in the Canadian Arctic.

Richard B. Langley is a professor in the Department of Geodesy and Geomatics Engineering at the University of New Brunswick (UNB) in Fredericton, Canada, where he has been teaching and conducting research since 1981. He has a B.Sc. in applied physics from the University of Waterloo and a Ph.D. in experimental space science from York University, Toronto.

John W. MacDougall is a professor Emeritus at the University of Western Ontario. He works on the development of digital ionosonde hardware and data processing algorithms for these instruments. His research focuses on ionospheric structure and morphology and its connections to space weather processes.